Published online 9 October 2020 *Nucleic Acids Research, 2020, Vol. 48, No. 19* **11083–11096**
doi: 10.1093/nar/gkaa816

METTL3 counteracts premature aging via m^{6}A-dependent stabilization of MIS12 mRNA

Zeming Wu[1,2,3,†], Yue Shi[3,4,5,†], Mingming Lu[3,4,5,†], Moshi Song[2,3,6], Zihui Yu[3,5], Jilu Wang[3,4,5], Si Wang[2,3,6,7], Jie Ren[2,3,4,5], Yun-Gui Yang[2,3,4,5], Guang-Hui Liu[2,3,6,7,*], Weiqi Zhang[2,3,4,5,*], Weimin Ci[2,3,4,5,*] and Jing Qu[1,2,3,*]

[1]State Key Laboratory of Stem Cell and Reproductive Biology, Institute of Zoology, Chinese Academy of Sciences, Beijing 100101, China, [2]Institute for Stem Cell and Regeneration, Chinese Academy of Sciences, Beijing 100101, China, [3]University of Chinese Academy of Sciences, Beijing 100049, China, [4]CAS Key Laboratory of Genomic and Precision Medicine, Beijing Institute of Genomics, Chinese Academy of Sciences, Beijing 100101, China, [5]China National Center for Bioinformation, Beijing 100101, China, [6]State Key Laboratory of Membrane Biology, Institute of Zoology, Chinese Academy of Sciences, Beijing 100101, China and [7]Advanced Innovation Center for Human Brain Protection, and National Clinical Research Center for Geriatric Disorders, Xuanwu Hospital Capital Medical University, Beijing 100053, China

Received June 27, 2020; Revised August 31, 2020; Editorial Decision September 15, 2020; Accepted September 23, 2020

ABSTRACT

N^6-Methyladenosine (m^{6}A) messenger RNA methylation is a well-known epitranscriptional regulatory mechanism affecting central biological processes, but its function in human cellular senescence remains uninvestigated. Here, we found that levels of both m^{6}A RNA methylation and the methyltransferase METTL3 were reduced in prematurely senescent human mesenchymal stem cell (hMSC) models of progeroid syndromes. Transcriptional profiling of m^{6}A modifications further identified *MIS12*, for which m^{6}A modifications were reduced in both prematurely senescent hMSCs and METTL3-deficient hMSCs. Knockout of *METTL3* accelerated hMSC senescence whereas overexpression of METTL3 rescued the senescent phenotypes. Mechanistically, loss of m^{6}A modifications accelerated the turnover and decreased the expression of *MIS12* mRNA while knockout of *MIS12* accelerated cellular senescence. Furthermore, m^{6}A reader IGF2BP2 was identified as a key player in recognizing and stabilizing m^{6}A-modified *MIS12* mRNA. Taken together, we discovered that METTL3 alleviates hMSC senescence through m^{6}A modification-dependent stabilization of the *MIS12* transcript, representing a novel epitranscriptional mechanism in premature stem cell senescence.

INTRODUCTION

Reversible N^6-methyladenosine (m^{6}A) mRNA modifications, one of the most abundant epitranscriptomic modifications, regulate transcriptional, post-transcriptional and translational mechanisms (1–5). Accordingly, the m^{6}A modification impinges on central biological processes such as stemness maintenance and differentiation, adipogenesis, and spermatogenesis, and its regulation impacts on pathological processes underlying obesity, infertility, neuronal disorders, aberrant immune signaling and cancers (6–10). Mechanistically, recent studies have revealed that m^{6}A regulates the formation and stability of R-loops, and promotes the phase separation potential of methylated mRNAs (2,11,12), thus providing novel insights into the regulatory role of m^{6}A modifications.

m^{6}A RNA modifications are deposited by a core methyltransferase complex composed of METTL3 and METTL14 and removed by demethylases ALKBH5 and FTO (4,13). As the core catalytic component in the methyltransferase complex (14,15), loss of METTL3 disrupts numerous physiological processes such as progression of spermatogenesis, hematopoiesis and memory formation (16–19). In addition, METTL3 functions as an oncogene in many types of cancers, while its ablation inhibits tumorigenic cell proliferation by affecting m^{6}A levels of target RNAs (20–22). The fate of m^{6}A-modified RNAs is then determined by m^{6}A readers, such as YTH family proteins, which affect their splicing, transport, stability, and translation (10,13). In addition, IGF2BP family members, including IGF2BP1, IGF2BP2,

*To whom correspondence should be addressed. Tel: +86 10 64807768; Email: qujing@ioz.ac.cn
Correspondence may also be addressed to Weimin Ci. Tel: +86 10 84097318; Email: ciwm@big.ac.cn
Correspondence may also be addressed to Weiqi Zhang. Tel: +86 10 84097843; Email: zhangwq@big.ac.cn
Correspondence may also be addressed to Guang-Hui Liu. Tel: +86 10 64807852; Email: ghliu@ioz.ac.cn
†The authors wish it to be known that, in their opinion, the first three authors should be regarded as Joint First Authors.

and IGF2BP3, may also function as m^{6}A readers to enhance the stability of target mRNAs, thus affecting gene expression outputs as a consequence of normal and stress conditions (23). Overall, this body of work frames a complex regulatory network role for m^{6}A in fundamental cell biological processes. However, the role of m^{6}A RNA modifications in cellular senescence remains largely unknown.

Premature aging diseases, also named as progeroid syndromes, are rare human disorders characterized by accelerated features of normal human aging, such as hearing loss, alopecia, lipodystrophy, osteoporosis and atherosclerosis (24–28). Of these progerias, Hutchinson-Gilford progeria syndrome (HGPS) and Werner syndrome (WS) are two of the best characterized. HGPS is characterized by progerin accumulation caused by *LMNA* mutation, leading to dysmorphic nuclei, increased DNA damage, and loss of heterochromatin (29–31). WS is caused by mutations in the *WRN* gene that encodes a RecQ DNA helicase involved in DNA replication and DNA damage repair. Loss of WRN leads to genomic instability that contributes to accelerated cellular senescence (29,32–34). Dysfunction of transcription, translation, replication, and chromatin organization have been described during the premature aging process (32,35–40). In addition, epigenetic dysregulation has been widely characterized in premature aging, and epigenetic reprogramming has even been suggested as a promising strategy for aging rejuvenation (31,41,42), raising the question whether epitranscriptomic modifications, such as m^{6}A RNA methylations, directly regulate premature aging.

Here, we employed isogenic human mesenchymal stem cells (hMSCs) with *LMNA* mutation and *WRN* knockout as HGPS and WS models (29), respectively, to explore the function of m^{6}A RNA modifications in the regulation of premature stem cell aging. We found that decreased m^{6}A modifications were associated with downregulated METTL3 expression, and that hMSCs with *METTL3* knockout showed characteristics of accelerated senescence. Conversely, METTL3 overexpression increased m^{6}A modifications and alleviated senescent phenotypes in HGPS and WS hMSCs. To identify specific targets affected by the loss of m^{6}A modifications in premature aging, we conducted RNA sequencing (RNA-seq) and m^{6}A methylated RNA immunoprecipitation sequencing (MeRIP-seq) analyses, and identified MIS12 as a key m^{6}A effector, whose deficiency accelerated hMSC senescence. Mechanistically, we discovered that the m^{6}A reader IGF2BP2 recognized and stabilized m^{6}A-modified *MIS12* mRNA to prevent hMSCs from accelerated senescence. Our findings provide novel insights into epitranscriptional mechanisms underpinning stem cell senescence via m^{6}A modifications and identify a potential intervention strategy for the treatment of aging-associated disorders.

MATERIALS AND METHODS

Antibodies

Antibodies used for western blotting, dot blotting, immunostaining or RNA immunoprecipitation (RIP): anti-m^{6}A (Synaptic Systems, 202003), anti-METTL3 (Proteintech, 15073-1-AP), anti-METTL14 (Sigma, HPA038002), anti-MIS12 (Abcam, ab70843), anti-IGF2BP2 (Bethyl Laboratories, A303–317A), anti-β-Tubulin (Santa Cruz, sc-5274), anti-GAPDH (Santa Cruz, sc-25778), anti-β-Actin (Santa Cruz, sc-69879), horseradish peroxidase (HRP)-conjugated secondary antibodies (ZSGB-BIO, ZB2305 and ZB2301), Alexa Fluor 488 donkey anti-mouse IgG (Invitrogen, A21202), Alexa Fluor 568 donkey anti-rabbit IgG (Invitrogen, A10042).

Cell culture

hMSC differentiation was performed as previously reported (29). All hMSCs were cultured in MSC culture medium: 90% α-MEM with GlutaMAX (Gibco), 10% fetal bovine serum (FBS, Gemcell, Cat# 100–500, Lot# A77E01F), 0.1 mM non-essential amino acids (NEAA, Gibco), 1% penicillin/streptomycin (Gibco) and 1 ng/ml FGF2 (Joint Protein Central).

Clonal expansion assay

The single-cell clonal expansion assay was carried out as previously described (29). Briefly, 2000 cells were seeded in a gelatin-coated 12-well plate (Corning Incorporated). About 10 days later, the cells were fixed with 4% paraformaldehyde for 30 min and stained with 0.2% crystal violet for 30 min at room temperature. Images were captured with an optical scanner (Hewlett-Packard). The relative cell density was determined using ImageJ.

Senescence-associated-β-galactosidase (SA-β-Gal) staining

SA-β-Gal staining was performed as previously described (29). Briefly, cultured cells were washed twice with PBS and fixed at room temperature for 5 min in 2% formaldehyde and 0.2% glutaraldehyde. Fixed cells were stained with SA-β-Gal staining solution (40 mM citric acid/Na phosphate buffer, 5 mM $K_4[Fe(CN)_6]$, 5 mM $K_3[Fe(CN)_6]$, 150 mM NaCl, 2 mM $MgCl_2$, 1 mg/ml X-gal) at 37°C overnight, and images were captured using a microscope digital camera (Olympus). The percentage of SA-β-Gal-positive cells were calculated with ImageJ.

m^{6}A dot blotting assay

Dot blotting assay was performed as previously reported (2,43). Briefly, total RNA was extracted using TRIzol reagent (Invitrogen). mRNA was prepared from total RNA using the Dynabeads mRNA Purification Kit (Life Technologies, 61006). 100–200 ng of mRNA was used for dot blot analysis using an antibody specific for m^{6}A. The results of dot blotting were obtained using ChemiDoc XRS system (Bio-Rad) and quantified by ImageJ. Methylene blue (MB) staining was used as loading control.

Western blotting

For western blotting, as previously reported (29), cells were lysed in RIPA buffer with the protease inhibitor cocktail (Roche). Protein lysates were quantified with a BCA quantification kit (Thermo Fisher Scientific), subjected to SDS-PAGE and electrotransferred to PVDF membranes (Millipore). Membranes were then blocked with 5% non-fat

milk in TBST (20 mM Tris–HCl, pH 7.5, 140 mM NaCl, 0.1% Tween-20), incubated with primary antibodies, followed by incubation with HRP-conjugated secondary antibodies. Western blotting results were obtained using Chemi-Doc XRS system (Bio-Rad), and quantification was performed with ImageJ.

Immunofluorescence microscopy

Immunostaining was conducted as previously described (29). In brief, cells seeded on microscope coverslips were fixed with 4% paraformaldehyde for 30 min, permeabilized with 0.4% Triton X-100 in PBS for 25 min, and blocked with 10% donkey serum in PBS for 1 h at room temperature. The coverslips were incubated with the primary antibody (diluted with 1% donkey serum in PBS) overnight at 4°C, and then incubated with the fluorescence-labeled secondary antibody (diluted with 1% donkey serum in PBS at 1:500) at room temperature for 1 h. Hoechst 33342 (Invitrogen) was used to stain nuclear DNA. Images were captured with a confocal system (Leica SP5).

Reverse transcription and quantitative PCR (RT-qPCR)

Total RNA was extracted using TRIzol reagent (Invitrogen). 2 μg of RNA was converted to cDNA by using the GoScript Reverse Transcription System (Promega), and 1/100 volume of the cDNA was applied to qPCR. qPCR was performed by using iTaq Universal SYBR Green Supermix (TOYOBO). RT-qPCR primers are listed in Supplementary Table S1.

m^{6}A methylated RNA immunoprecipitation assay (m^{6}A-RIP/MeRIP)

The procedure of m^{6}A immunoprecipitation (m^{6}A-RIP or MeRIP) was modified from previously reported methods (44,45). In brief, purified mRNA was digested by DNase I and then fragmented into ∼100 nt in length by a 45-s incubation at 94°C in RNA fragmentation reagent (Life Technologies, AM8740). The reaction was stopped with a stop buffer (Life Technologies, AM8740), followed by standard ethanol precipitation and collection. 12 μg of anti-m^{6}A antibody was pre-incubated with 50 μl Protein A Dynabeads (Life Technologies, 10013D) in IPP buffer (150 mM NaCl, 0.1% NP-40, 10 mM Tris–HCl, pH 7.4) for 1 h at room temperature. After pre-heating at 75°C for 5 min and chilling on ice immediately, 6 μg of fragmented mRNAs were added to the above prepared antibody-beads mixture and incubated for 4 h at 4°C on a rotator. After extensive washing, immunoprecipitated mixture were digested by proteinase K, and bound RNAs were subjected to phenol-chloroform (Life Technologies, AM9730) extraction and ethanol precipitation and then used for library construction or RT-qPCR analysis. The library constructions of IP-RNA samples were performed using a SMARTer smRNA-Seq Kit (Takara, 635030) and a small fraction of fragmented mRNAs (input) before IP were subjected to RNA-seq using a KAPA Stranded RNA-Seq Library Preparation Kit (KAPA, KK8401) according to the manufacturer's instructions, and sequenced on the Illumina HiSeq X Ten platform.

IGF2BP2 RIP-qPCR

RIP was performed as previously described (46–48) with some modifications. Briefly, cells seeded in a 15-cm dish at 80–90% confluency were harvested in cold PBS by the cell lifter (Corning Incorporated), pelleted by centrifuge for 5 min at 1000 × *g* (at 4°C) and washed once with cold PBS. The cell pellet was re-suspended with 400 μl lysis-IP buffer (50 mM Tris–HCl, pH 7.4, 150 mM NaCl, 5 mM $MgCl_2$, 0.5% NP-40, 1 mM DTT, 1:100 protease inhibitor cocktail (Roche), 400 U/ml RNase inhibitor (Promega)), and incubated at 4°C for 2 h on a rotator and then centrifuged for 15 min to obtain clear lysates. One-tenth volume of the supernatant was saved as input and total RNA was extracted using TRIzol reagent. The remaining supernatant was incubated with IgG-conjugated protein A Dynabeads (Life Technologies) precoated with or without the anti-IGF2BP2 antibody in 500 μl lysis-IP buffer at 4°C overnight. After washing with lysis-IP buffer for five times, beads were re-suspended in 300 μl elution buffer (5 mM Tris–HCl, pH 7.5, 1 mM EDTA, pH 8.0, 0.05% SDS, 4 μl proteinase K (New England Biolabs)) and digested at 55°C for 1 h. Co-immunoprecipitated RNAs were obtained after digestion by phenol–chloroform extraction and ethanol precipitation and then analyzed by RT-qPCR.

RNA stability analysis

Assay for RNA stability analysis was performed as previously described (23,49) with some modifications. hMSCs were cultured in six-well culture plates (Corning Incorporated) to ∼80% confluence. Actinomycin D (ACTD, J&K Scientific) was added at a final concentration of 5 μg/ml. Cells were collected at five time points (0, 2, 4, 6, 8 h) after the addition of ACTD and total RNA was extracted with TRIzol reagent. RT-qPCR was performed as above and *GAPDH* was used as loading control for normalization. For each RNA transcript of interest, a semi-log graph was plotted and its RNA half-life ($t_{(1/2)}$) was determined in each condition tested.

Liquid chromatography-tandem mass spectrometry (LC-MS/MS)

LC–MS/MS analysis was conducted as previously reported (49–51). In brief, 100–200 ng of mRNA was digested by 0.1 U Nuclease P1 (Sigma) and 1.0 U calf intestinal phosphatase (New England Biolabs) in a final reaction volume of 50 μl, adjusted with water and incubated at 37°C overnight. The sample was then filtered (MW cutoff: 3 kDa, Pall, Port Washington) and subjected to LC–MS/MS analysis for detection of m^{6}A. The nucleosides were separated by reverse phase ultra-performance liquid chromatography on a C18 column with online mass spectrometry detection using a G6410B triple quadrupole mass spectrometer (Agilent Technologies) in the positive ion mode. The nucleosides were quantified by using the nucleoside-to-base ion mass transitions of *m/z* 282 to 150 (m^{6}A) and *m/z* 268 to 136 (A). Quantification was carried out by comparison with a standard curve obtained from pure nucleoside standards run with the same batch of samples. The ratio of m^{6}A to A was calculated based on the calibrated concentrations.

Plasmid construction

For the construction of overexpression (OE) plasmids, cDNA prepared by reverse transcription of RNA from hMSCs was used as template to amplify genes of interest. Sequence information of full-length human *METTL3* (Gene ID: NM_019852.5) was obtained from NCBI (https://www.ncbi.nlm.nih.gov/). cDNA of *METTL3* was cloned into vector pLE4 (a kind gift from Dr Tomoaki Hishida) and pLE4-*Luc* (Luciferase) was used as control.

For lentiviral CRISPR/Cas9-mediated knockout, the sgRNA targeting *METTL3* or *MIS12* was cloned into the lenti-CRISPRv2 (Addgene, #52961) vector with an hSpCas9 expression cassette.

For lentiviral shRNA-mediated knockdown, the shRNA targeting *IGF2BP2* was cloned into the pLVTHM vector (Addgene, #12247).

All the primers used for cloning are listed in Supplementary Table S1.

Lentivirus packaging

For lentivirus packaging, HEK293T cells were co-transfected with lentiviral vectors, psPAX2 (Addgene, #12260) and pMD2G (Addgene, #12259) using VigoFect Transfection Reagent (Vigorous Biotechnology). Viral particles were collected by ultracentrifugation at 19 400 $\times$ *g* at 4°C for 2.5 h.

Lentiviral CRISPR/Cas9-mediated gene knockout and lentiviral shRNA-mediated gene knockdown

Lentiviral CRISPR/Cas9-mediated gene knockout and lentiviral shRNA-mediated knockdown were conducted as previously described (52,53). Lentiviruses packaged with pLenti-CRISPRv2-*METTL3*, pLenti-CRISPRv2-*MIS12* or pLVTHM-*IGF2BP2* were transduced into WT-hMSCs. Lentiviruses containing pLenti-CRISPRv2-NTC (non-targeting control) or pLVTHM-CTRL (control) were used as negative controls. For lentiviral CRISPR/Cas9-mediated gene knockout, 48 h post-transfection, cells were treated with puromycin (Thermo Fisher Scientific) for screening with serial passaging. Phenotypic analyses were conducted after two passages.

RNA-seq

Total RNA was extracted using TRIzol reagents from 1 $\times$ 10^6 cells per duplicate and genomic DNA removed using a DNA-free Kit (Thermo Fisher Scientific). Library construction was conducted using a KAPA Stranded RNA-Seq Library Preparation Kit (KAPA, KK8401) according to the manufacturer's instructions. Quality control and sequencing were performed by Novogene Bioinformatics Technology Co., Ltd.

Bioinformatic analysis

General read preprocessing: two biological replicates for each condition were performed. Adaptor sequences were trimmed off for all raw reads using the FASTX_toolkit (version 0.0.14). Reads that were less than 35 nt in length or containing an ambiguous nucleotide were discarded by Trimmomatic (version 0.36). The remaining reads were aligned to the human reference genome (hg19) using HISAT2 (version 2.1.0). Only uniquely mapped reads with mapping quality score $\geq$20 were kept for the subsequent analysis of each sample.

For MeRIP-seq: the m^{6}A peaks were called using the MACS2 peak-calling software (version 2.1.2) with the default options except for '–nomodel,–keepdup all'. A stringent cutoff threshold for a *P*-value of 1×10^{-5} and an enrichment score of 3 were used to obtain high-confidence peaks. Each peak was annotated based on the UCSC gene annotation information by applying BEDTools 'IntersectBed' (version 2.25.0). Motif enrichment was analyzed by HOMER selecting a motif length of 6 nucleotides. Background regions were generated by shuffling peaks along the transcriptome using the shuffleBed tool from the BEDTools software.

For RNA-seq: the number of uniquely mapped reads was counted using the HTSeq python package (version 0.9.1). The expression of genes was quantified as reads per kilobase of exon model per million mapped reads (RPKM). Differentially expressed genes between WT and HGPS hMSCs, WS hMSCs, or between control and *METTL3*-knockout hMSCs were determined using the R-package DEseq2 software (fold-change cutoff = 2.0, *P*-value cutoff = 5×10^{-2}).

For functional enrichment analysis: Gene ontology (GO) analysis of genes with m^{6}A modification or with differential expression was performed using metascape (http://metascape.org) or ClusterProfiler, an R package that analyzes and visualizes functional profiles (GO or KEGG) of genes and gene clusters. GO terms with a *P*-value $<$ 0.05 were set to be statistically significant.

Statistical analysis

Results were presented as mean $\pm$ SEM. Two-tailed Student's *t*-test was conducted by using the Graph-Pad Prism Software. *P*-values $<$ 0.05, *P*-values $<$ 0.01 and *P*-values $<$ 0.001 were considered statistically significant (marked with *, **, ***, respectively).

RESULTS

Decreased mRNA m^{6}A modifications in HGPS and WS hMSCs

Here, we leveraged premature aging cellular models, including HGPS hMSCs (with heterozygous (G608G/+) or homozygous (G608G/G608G) *LMNA* mutation) and WS hMSCs (with a biallelic *WRN* knockout) (29,31,32,54–56), to reveal unknown aspects of m^{6}A biology as a consequence of aging. Premature aging phenotypes were first validated (Figure 1A–C). Subsequently, m^{6}A-specific dot blot analysis revealed a significant reduction of m^{6}A levels in HGPS and WS hMSCs (Figure 1D), as confirmed by both immunofluorescence microscopic analysis and liquid chromatography-tandem mass spectrometry (LC-MS/MS) (Figure 1E, F). Consistent with this observation, protein

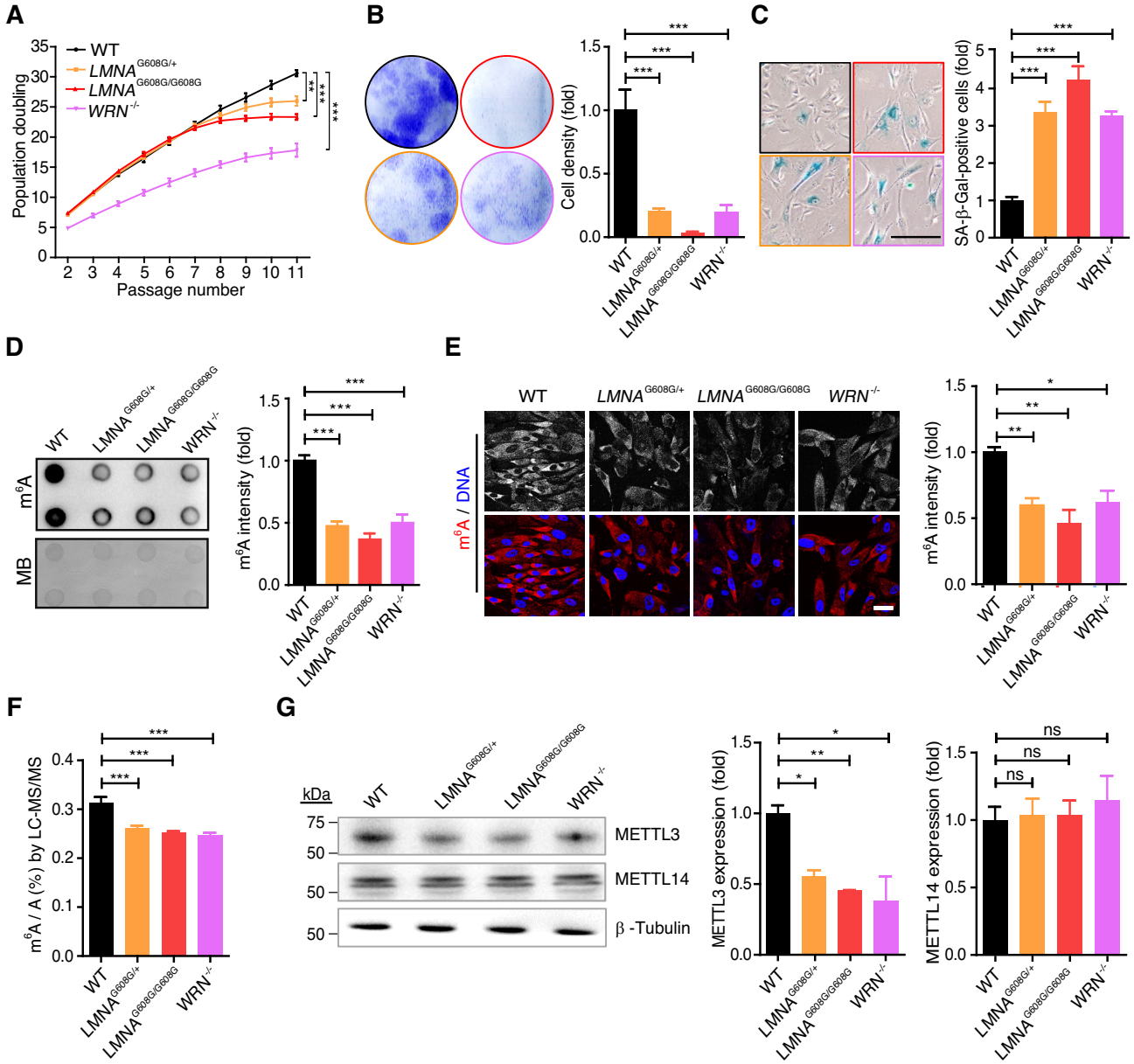

Figure 1. Reduced m^{6}A methylation in prematurely senescent hMSCs. (**A**) Growth curve analysis showing population doubling of WT, HGPS (*LMNA*$^{G608G/+}$, *LMNA*$^{G608G/G608G}$) and WS (*WRN*$^{-/-}$) hMSCs. Data are presented as means ± SEM, $n = 3$. Statistical significances are shown for passage 11. $^{**}P < 0.01$; $^{***}P < 0.001$. Subsequent biological analyses in prematurely senescent hMSCs were conducted at Passage 9. (**B**) Clonal formation assay in WT, HGPS and WS hMSCs. Data are presented as means ± SEM, $n = 3$. $^{***}P < 0.001$. (**C**) Analysis of SA-β-Gal activity in WT, HGPS and WS hMSCs. Scale bar, 200 μm. Data are presented as means ± SEM, $n = 3$. $^{***}P < 0.001$. (**D**) Dot blot analysis of m^{6}A levels in mRNA extracted from the indicated hMSCs. Methylene blue (MB) staining was used as RNA loading control. Data are presented as means ± SEM. $^{***}P < 0.001$. (**E**) Immunostaining analysis of m^{6}A in WT, HGPS and WS hMSCs. Scale bar, 50 μm. Data are presented as means ± SEM, $n = 3$. $^{*}P < 0.05$; $^{**}P < 0.01$. (**F**) LC–MS/MS analysis of m^{6}A levels in mRNA extracted from the indicated hMSCs. Data are presented as means ± SEM, $n = 3$. $^{***}P < 0.001$. (**G**) Western blot analysis of expression of core m^{6}A methyltransferases in WT, HGPS and WS hMSCs. β-Tubulin was used as loading control. Data are presented as means ± SEM, $n = 3$. $^{*}P < 0.05$; $^{**}P < 0.01$; ns, not significant.

levels of METTL3 were also reduced in HGPS and WS hMSCs (Figure 1G). By comparison, we did not detect any significant alterations in the expression of another m^{6}A methyltransferase, METTL14 (Figure 1G). Taken together, these results suggest that decreased METTL3 expression may contribute to m^{6}A loss in prematurely aged hMSCs.

METTL3 is indispensable for preventing hMSCs from accelerated senescence

Similarly to broadly related studies using a loss of function approaches to probe functional roles of METTL3 (5,6,14,15), we knocked out *METTL3* in WT hMSCs using a CRISPR/Cas9-based method (Figure 2A and

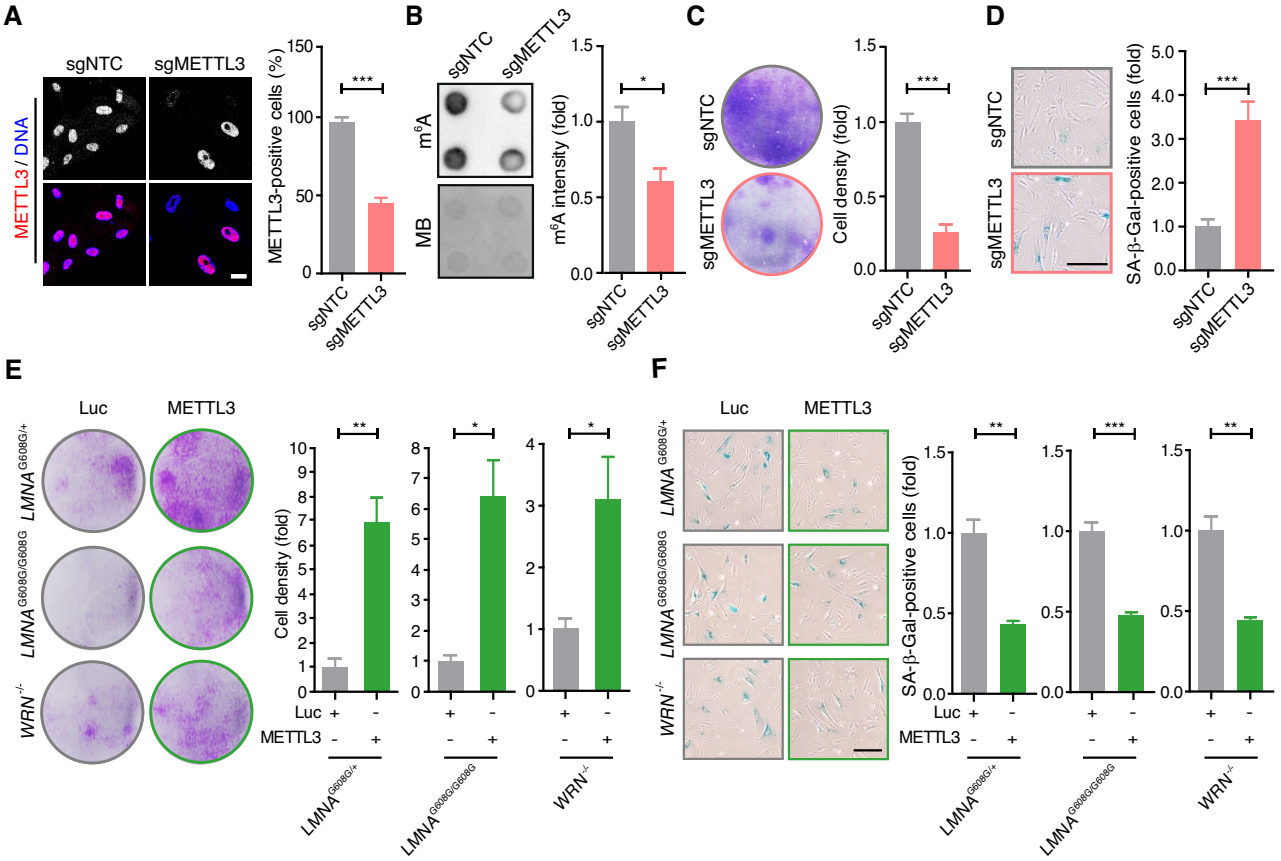

Figure 2. Loss of METTL3 induces senescence in hMSCs while METTL3 overexpression reverses senescence in prematurely senescent hMSCs. (**A**) Immunostaining analysis of METTL3 in control (sgNTC) and *METTL3*-knockout (sgMETTL3) hMSCs. Scale bar, 20 μm. Data are presented as means ± SEM, $n = 3$. ***$P < 0.001$. (**B**) Dot blot analysis of m^{6}A mRNA modification in control and *METTL3*-knockout hMSCs. Methylene blue staining was used as RNA loading control. Data are presented as means ± SEM. *$P < 0.05$. (**C**) Clonal formation assay of control and *METTL3*-knockout hMSCs. Data are presented as means ± SEM, $n = 3$. ***$P < 0.001$. (**D**) SA-β-Gal staining of control and *METTL3*-knockout hMSCs. Scale bar, 200 μm. Data are presented as means ± SEM, $n = 3$. ***$P < 0.001$. (**E**) Clonal formation assay of hMSCs overexpressing Luc or METTL3. Data are presented as means ± SEM, $n = 3$. *$P < 0.05$; **$P < 0.01$. (**F**) SA-β-Gal staining of hMSCs overexpressing Luc or METTL3. Scale bar, 200 μm. Data are presented as means ± SEM, $n = 3$. **$P < 0.01$; ***$P < 0.001$.

Supplementary Figure S1A). Knockout of *METTL3* (sgMETTL3) led to decreased m^{6}A modification levels as compared to those in control hMSCs (sgNTC) (Figure 2B and Supplementary Figure S1B). Furthermore, METTL3-deficient hMSCs acquired premature aging phenotypes, as evidenced by decreased proliferative capacity and increased percentage of SA-β-Gal-positive cells (Figure 2C, D). These results suggest that METTL3 deficiency accelerates hMSC senescence.

To investigate whether increased m^{6}A might delay the onset of premature senescence in progeria hMSCs, we overexpressed METTL3 in HGPS and WS hMSCs. As expected, overexpression of METTL3 increased global m^{6}A modification levels (Supplementary Figure S1C, D). Moreover, enhanced cell proliferative capacity and reduced SA-β-Gal-positive cells were observed in HGPS and WS hMSCs upon METTL3 overexpression (Figure 2E, F). Collectively, these results suggest that intact METTL3 function is important for staving off senescence in hMSCs.

Transcriptome-wide profiling of m^{6}A modifications in WT and prematurely aged hMSCs

We next performed RNA-seq and MeRIP-seq in HGPS and WS hMSCs to depict a transcriptome-wide m^{6}A landscape in premature aging (Supplementary Figure S2A-B). High reproducibility was confirmed by examining Pearson's correlation coefficients between replicates of each condition. And >10 000 m^{6}A peaks in overlapping regions for each pair of independent replicates were detected, demonstrating the high quality of MeRIP-seq data (Supplementary Figure S2A–C). Further analysis revealed that m^{6}A modifications were mainly found in the protein-coding mRNAs (Supplementary Figure S2D), typically located in a consensus 'DRACH' motif (D = A/G/U; R = A/G; and H = U/A/C) (Figure 3A) and also highly enriched in the coding sequence, 3′-untranslated regions (3′ UTR) and near the stop codons (Figure 3B and Supplementary Figure S2E) as previously reported (50,57,58).

We integrated the RNA-seq analysis with the MeRIP-seq analysis and revealed that transcripts with m^{6}A modifica-

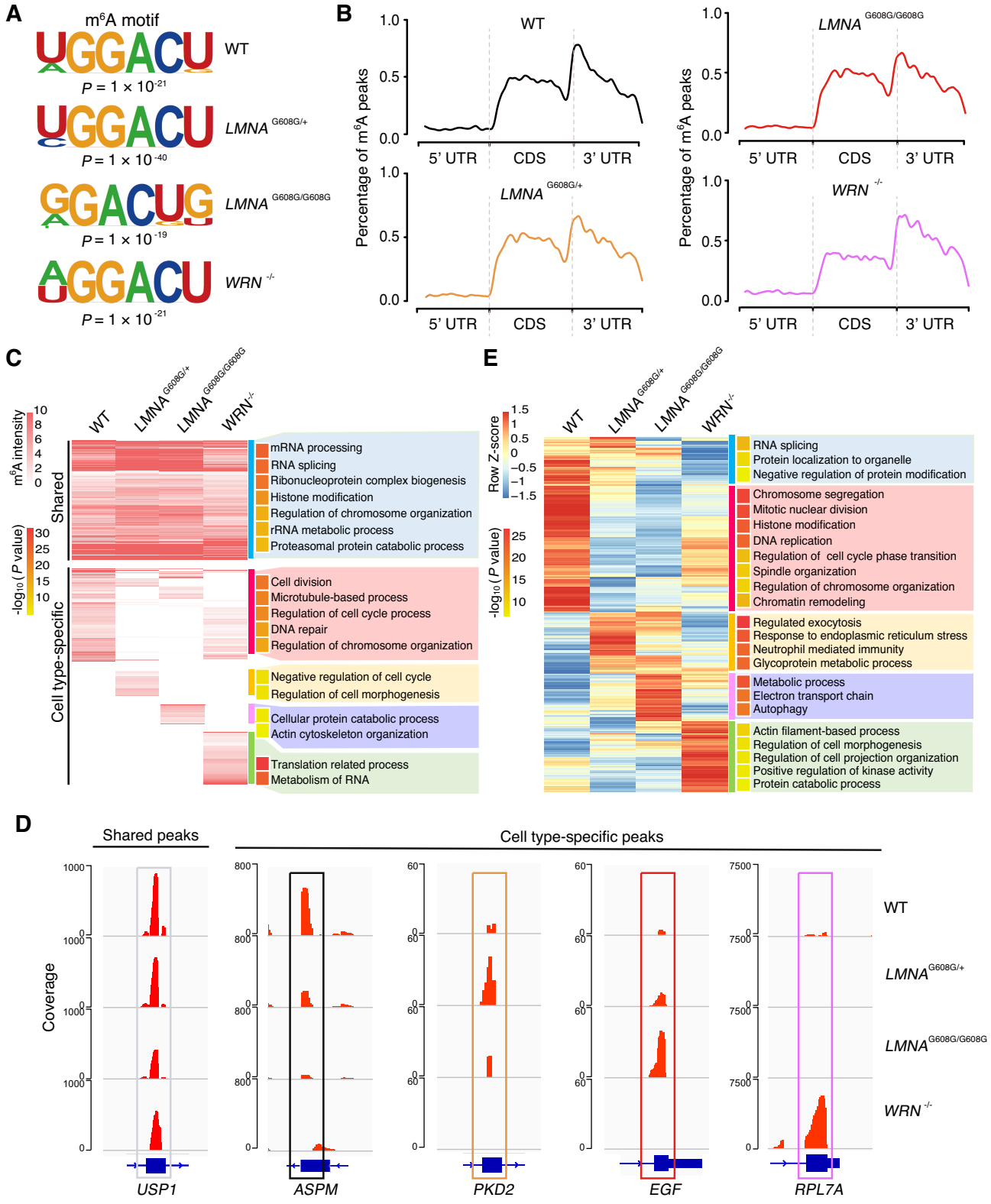

Figure 3. m^{6}A profiling in prematurely senescent hMSCs. (**A**) m^{6}A motif identified in WT, HGPS and WS hMSCs. (**B**) Distribution of m^{6}A peaks along the 5′ UTR, CDS, and 3′ UTR regions of total mRNA from each cell line normalized for length. (**C**) Heatmap showing shared and specific m^{6}A peaks in the indicated hMSCs. The colour key (up) from light to dark represents m^{6}A enrichment from low to high. GO analysis is shown on the right. The colour key (down) from yellow to red indicates -log$_{10}$ (*P* value) from low to high. (**D**) IGV plots showing examples of shared and specific m^{6}A peaks. Peaks are represented as subtracted read densities (IP minus input). (**E**) Heatmap showing clustering of differentially expressed genes in prematurely senescent hMSCs relative to WT-hMSCs. The colour key (up) from blue to red represents scaled expression values from low to high. GO analysis is shown on the right. The colour key (down) from yellow to red indicates -log$_{10}$ (*P* value) from low to high.

tions were overall more highly expressed than transcripts without m^{6}A modifications (Supplementary Figure S3A), pointing to a potential regulatory role of m^{6}A in gene expression homeostasis. We then subdivided all the transcripts according to their expression levels and found m^{6}A modification levels were positively associated with mRNA expression levels (Supplementary Figure S3B). Furthermore, we noticed that the expression of mRNAs with reduced m^{6}A modifications as a consequence of premature senescence was downregulated, while upregulated mRNAs were correlated with the gain of m^{6}A modifications (Supplementary Figure S3C), and that this correlation occurred across different regions of the transcripts (Supplementary Figure S3D). Altogether, our data suggest a positive correlation between m^{6}A modification levels and mRNA expression levels, consistent with previous study (59).

Reduced mRNA m^{6}A methylation in cell cycle-related genes during hMSC senescence

To understand the biological relevance of m^{6}A modifications in premature senescence, we investigated shared and cell type-specific m^{6}A peaks in WT, HGPS and WS hMSCs (Figure 3C, D). Transcripts with shared m^{6}A peaks (such as *USP1*) were mainly enriched for mRNA processing, RNA splicing, and histone modification pathways (Figure 3C, D), most of which are essential for cell survival (60–64). By contrast, transcripts with m^{6}A peaks specific for premature aging models were enriched for cell morphogenesis, cellular protein catabolic process and actin cytoskeleton organization in HGPS hMSCs, such as *PKD2* and *EGF* (Figure 3C, D), and translation-related process and RNA metabolism in WS hMSCs, such as *RPL7A* (Figure 3C, D). Consistent with our data showing a global loss of mRNA methylation in premature aging cell models (Figure 1D–F), m^{6}A modifications were decreased in all three hMSC senescence models relative to those in WT hMSCs (Figure 3C). Moreover, the premature senescence-associated hypomethylated transcripts that harbored WT-specific m^{6}A peaks were involved in functional categories related to cell division, microtubule-based process, regulation of cell cycle, DNA repair and chromosome organization (Figure 3C), such as *ASPM* (Figure 3D). Most of these terms are cell cycle-related pathways, which are dysregulated during aging (65–67).

Next, we investigated gene expression profiles of WT, HGPS and WS hMSCs and found distinct patterns in each cell line (Figure 3E and Supplementary Figure S4A-D). The gene expression patterns of heterozygous and homozygous HGPS hMSCs were similar to each other, but were largely different from those of WT and WS hMSCs. In HGPS hMSCs, highly expressed genes were related to exocytosis, endoplasmic reticulum stress, immune responses, metabolic processes and autophagy (Figure 3E). In WS hMSCs, pathways regulating actin filament-based processes, cell morphogenesis, cell projection organization, kinase activities, as well as protein catabolic processes, were significantly enriched with highly expressed genes (Figure 3E). In addition, we found the genes upregulated in both HGPS and WS hMSCs were enriched in developmental pathways (Supplementary Figure S4A, B). By comparison, highly expressed genes in WT hMSCs (also representing downregulated genes in premature senescence) were enriched in chromosome segregation, nuclear division, histone modification, DNA replication, cell cycle phase transition and spindle organization pathways (Figure 3E and Supplementary Figure S4C-D), most of which were cell cycle-related terms as aforementioned (Figure 3C). These data suggest that cell cycle-related genes showing m^{6}A loss and downregulated expression may play predominant roles in regulating hMSC senescence.

We next compared the m^{6}A profiles in METTL3-deficient and control hMSCs (Supplementary Figure S5A–E) and observed similar patterns to those of WT and prematurely senescent hMSCs. Shared m^{6}A-modified transcripts between METTL3-deficient and control hMSCs were mainly enriched in histone modification and RNA processing pathways (Supplementary Figure S5F, G). We also noticed the presence of a small fraction of transcripts with increased m^{6}A modifications after METTL3 deletion (Supplementary Figure S5F, G), likely due to the existence of other m^{6}A methyltransferases. Notably, regulation of cell cycle progression was also enriched for transcripts showing m^{6}A loss after *METTL3* knockout (Supplementary Figure S5F, G), in further support of altered m^{6}A modifications in cell cycle-related genes potentially contributing to hMSC senescence.

MIS12 functions as a key m^{6}A target in premature senescence

In search for key regulators mediating m^{6}A-associated effects in hMSC senescence, we discovered a common loss of mRNA methylations near the stop codons of transcripts both in prematurely senescent and METTL3-deficient hMSCs (Figure 4A, B and Supplementary Figure S6A–D). GO analysis of these transcripts revealed enrichment of cell cycle-related terms (Figure 4C) as described above. Among these transcripts, we noticed that m^{6}A modifications in *MIS12*, a key regulator of cell proliferation (68), were markedly reduced in both prematurely senescent and METTL3-deficient hMSCs (Figure 4D and Supplementary Figure S6E), as validated by MeRIP-qPCR analysis (Figure 4E, F). We also detected a significant decrease in MIS12 expression at both the mRNA and protein levels in HGPS and WS hMSCs as well as in METTL3-deficient hMSCs (Figure 5A–D).

When we examined the stability of *MIS12* mRNA, we observed a shortened mRNA half-life of *MIS12* in HGPS and WS hMSCs as well as in METTL3-deficient hMSCs (Supplementary Figure S7A, B), indicating that m^{6}A modifications may promote *MIS12* mRNA stability. Interestingly, a recent study has reported that IGF2BPs recognize m^{6}A modifications in thousands of mRNA transcripts and promote the stability and translation of these mRNAs, including *MIS12* identified as one of the targets of IGF2BP2 by high-throughput sequencing analyses (23). Accordingly, we asked whether IGF2BP2 recognition and stabilization of m^{6}A-modified *MIS12* mRNA might regulate hMSC senescence.

To test this hypothesis, we conducted RIP-qPCR analysis with an anti-IGF2BP2 antibody to detect a poten-

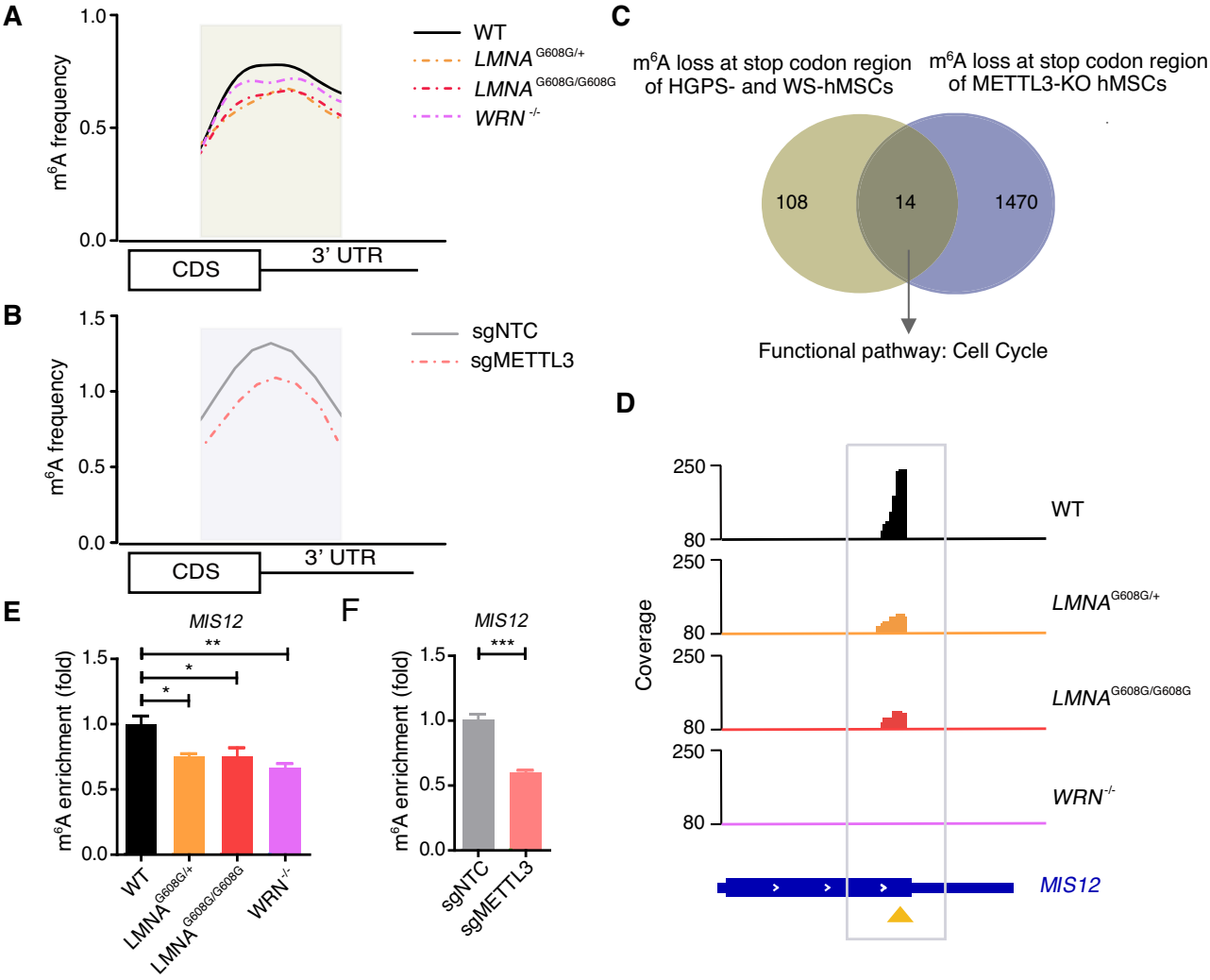

Figure 4. MIS12 is a downstream target of METTL3 that regulates hMSC senescence. (**A**) m^{6}A frequency near stop codon regions in transcripts from WT-, HGPS- and WS-hMSCs. (**B**) m^{6}A frequency near stop codon regions in transcripts from control and *METTL3*-knockout hMSCs. (**C**) Pie chart showing genes with m^{6}A loss at stop codon region that overlap between prematurely senescent hMSCs and *METTL3*-knockout hMSCs. (**D**) IGV plots showing m^{6}A modification on *MIS12* mRNA in different cell lines. Peaks are represented as subtracted read densities (IP minus input). White arrows indicate the direction of gene transcription and yellow triangle indicates the location of the m^{6}A peak. (**E**) MeRIP-qPCR detection for m^{6}A enrichment on *MIS12* mRNA of WT-, HGPS- and WS-hMSCs. Data are presented as means ± SEM, $n = 6$. *$P < 0.05$; **$P < 0.01$. (**F**) MeRIP-qPCR detection for m^{6}A enrichment on *MIS12* mRNA of control and *METTL3*-knockout hMSCs. Data are presented as means ± SEM, $n = 6$. ***$P < 0.001$.

tial interaction between IGF2BP2 and *MIS12* mRNA in hMSCs. Indeed, we observed a significantly higher enrichment of IGF2BP2 on *MIS12* mRNA relative to IgG control (Figure 5E). Importantly, METTL3 deficiency disrupted this interaction (Figure 5F), implying that IGF2BP2 binds *MIS12* mRNA in an METTL3/m^{6}A-dependent manner. To confirm that IGF2BP2 promotes MIS12 expression, we knocked down IGF2BP2 with shRNA in WT hMSCs and detected a significant decrease in MIS12 expression at both the mRNA and protein levels (Figure 5G–I). We also observed a shortened *MIS12* mRNA half-life after IGF2BP2 knockdown (Supplementary Figure S7C), suggesting that IGF2BP2 could recognize and stabilize m^{6}A-tagged *MIS12* mRNA.

Finally, we used a CRISPR/Cas9-based method to ablate *MIS12* in WT hMSCs (Figure 5J). As expected, MIS12 deficiency accelerated hMSC senescence, as evidenced by decreased proliferative capacity and increased SA-β-Gal staining (Figure 5K, L). Likewise, IGF2BP2 knockdown also led to accelerated cellular senescence in WT hMSCs (Figure 5M, N). Collectively, these data suggest that IGF2BP2 and its target mRNA *MIS12* contribute to m^{6}A-associated regulation of hMSC senescence.

DISCUSSION

Our results reveal that m^{6}A RNA modifications play a central role in regulating premature senescence in hMSCs. Firstly, we found that m^{6}A modification levels were reduced concomitant with the downregulation of METTL3 in prematurely senescent hMSCs. Secondly, the depletion of METTL3 led to reduced m^{6}A modifications and MIS12 downregulation, accelerating hMSC senescence. Thirdly, overexpression of METTL3 restored m^{6}A modifications

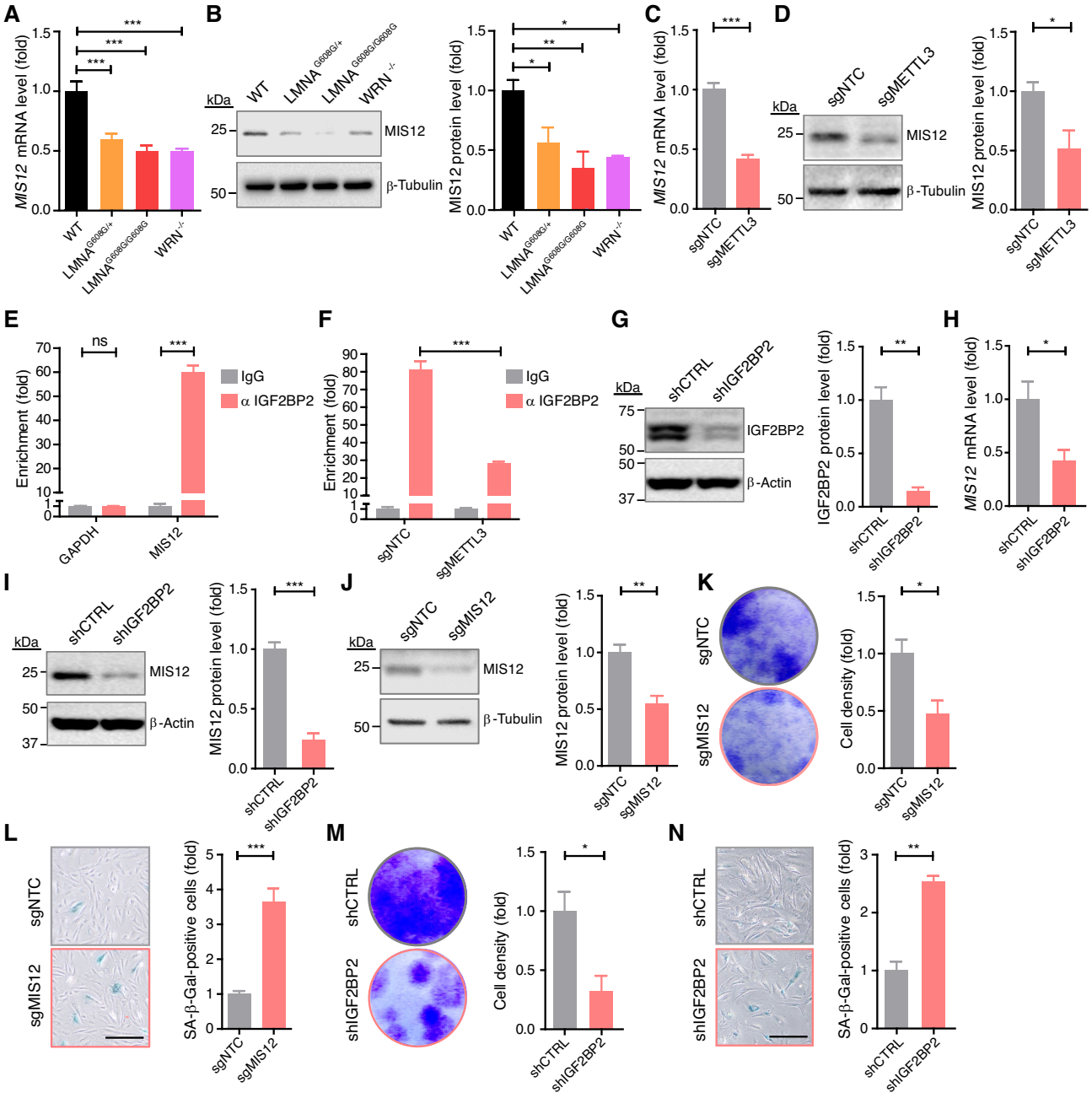

Figure 5. m^{6}A promotes IGF2BP2-mediated *MIS12* mRNA stability to prevent accelerated senescence in hMSC. (**A**) qPCR analysis of *MIS12* mRNA levels in WT, HGPS and WS hMSCs. Data are presented as means ± SEM, $n = 6$. ***$P < 0.001$. (**B**) Western blot analysis of MIS12 protein levels in WT, HGPS and WS hMSCs. β-Tubulin was used as loading control. Data are presented as means ± SEM, $n = 3$. *$P < 0.05$; **$P < 0.01$. (**C**) qPCR analysis of *MIS12* mRNA levels in control and *METTL3*-knockout hMSCs. Data are presented as means ± SEM, $n = 6$. ***$P < 0.001$. (**D**) Western blot analysis of MIS12 protein levels in control and *METTL3*-knockout hMSCs. β-Tubulin was used as loading control. Data are presented as means ± SEM, $n = 3$. *$P < 0.05$. (**E**) RIP-qPCR analysis showing enrichment of IGF2BP2 on *MIS12* mRNA in WT hMSCs. IgG was used as isotype control. *GAPDH* was used as a negative control. Data are presented as means ± SEM, $n = 3$. ***$P < 0.001$; ns, not significant. (**F**) RIP-qPCR analysis showing enrichment of IGF2BP2 on *MIS12* mRNA in control and *METTL3*-knockout hMSCs. IgG was used as isotype control. Data are presented as means ± SEM, $n = 3$. ***$P < 0.001$. (**G**) Western blot analysis of IGF2BP2 protein levels in control (shCTRL) and IGF2BP2-silenced (shIGF2BP2) hMSCs. β-Actin was used as loading control. Data are presented as means ± SEM, $n = 3$. **$P < 0.01$. (**H**) qPCR analysis of the *MIS12* mRNA levels in control and IGF2BP2-silenced hMSCs. Data are presented as means ± SEM, $n = 3$. *$P < 0.05$. (**I**) Western blot analysis of the MIS12 protein levels in control and IGF2BP2-silenced hMSCs. β-Actin was used as loading control. Data are presented as means ± SEM, $n = 3$. ***$P < 0.001$. (**J**) Western blot analysis of MIS12 protein levels in control (sgNTC) and *MIS12*-knockout (sgMIS12) hMSCs. β-Tubulin was used as loading control. Data are presented as means ± SEM, $n = 3$. **$P < 0.01$. (**K**) Clonal formation assay of control and *MIS12*-knockout hMSCs. Data are presented as means ± SEM, $n = 3$. *$P < 0.05$. (**L**) SA-β-Gal staining of control and *MIS12*-knockout hMSCs. Scale bar, 200 μm. Data are presented as means ± SEM, $n = 3$. ***$P < 0.001$. (**M**) Clonal formation assay of control and IGF2BP2-silenced hMSCs. Data are presented as means ± SEM, $n = 3$. *$P < 0.05$. (**N**) SA-β-Gal staining of control and IGF2BP2-silenced hMSCs. Scale bar, 200 μm. Data are presented as means ± SEM, $n = 3$. **$P < 0.01$.

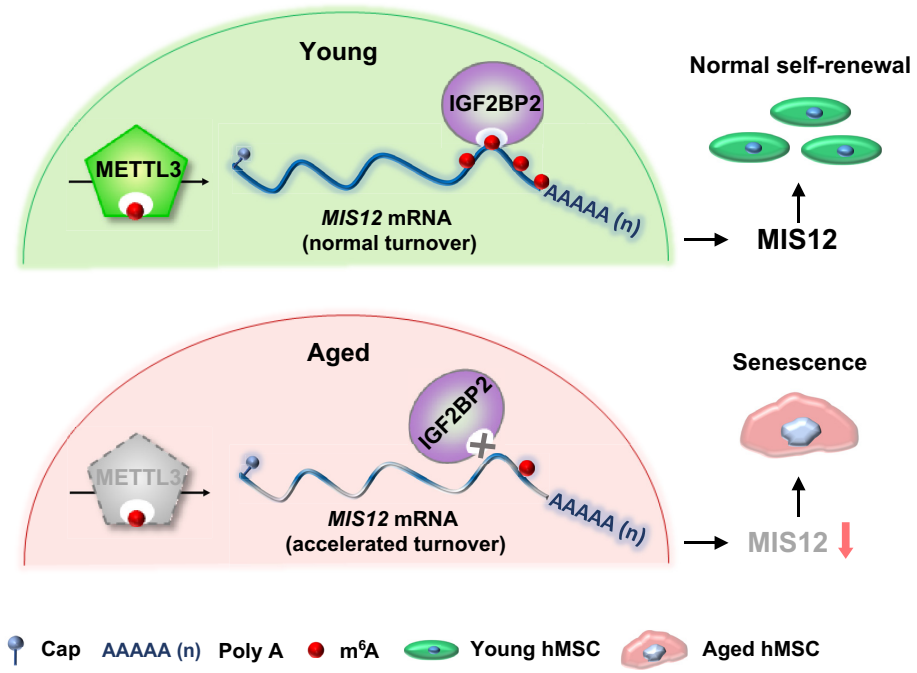

Figure 6. A model illustrating the protective role of METTL3/m^{6}A in alleviating hMSC senescence. In young cells, METTL3 maintains m^{6}A levels to stabilize *MIS12* mRNA; facilitating IGF2BP2 binding, MIS12 expression and hMSC self-renewal. In aged cells, METTL3 downregulation results in reduced m^{6}A levels; preventing IGF2BP2 binding and accelerating *MIS12* mRNA turnover, causing accelerated cellular senescence in hMSCs.

and prevented premature senescence in hMSCs. Finally, IGF2BP2 recognized and stabilized m^{6}A-modified *MIS12* mRNA to prevent accelerated hMSC senescence. Together, our findings demonstrate that METTL3 and m^{6}A modifications could alleviate hMSC senescence through IGF2BP2-mediated enhancement of *MIS12* mRNA stability (Figure 6), adding an epitranscriptional layer to the regulation of premature senescence in stem cells.

By targeting different mRNAs in different cell types and organs (13), m^{6}A regulation by METTL3 can shape biological processes in very different ways in both normal and diseased conditions. Aberrant m^{6}A modifications are known to lead to impaired embryonic development, tumorigenesis and the occurrence of diabetes by affecting the fate of specifically targeted mRNAs (21,69–71). Of significance for our findings, abnormal m^{6}A modifications are recently implicated in Parkinson's disease (PD) and Alzheimer's disease (AD) models, well-known age-related neurodegenerative disorders (72,73). Moreover, dysregulation of m^{6}A has also been implicated in age-related infertility and heart failure in mice (74,75). These findings all point to a regulatory role of m^{6}A in aging.

Consistent with our findings, Min *et al.* has reported that decreased m^{6}A modifications in human blood cells collected from aged individuals lead to cellular senescence in human fibroblasts, partially attributed to the instability of *AGO2* mRNA that may be recapitulated by METTL3 depletion (76). However, genetic differences between individuals were not investigated in this study, and a causal link between m^{6}A and aging has not yet been established. In our study, we employed isogenic wild-type and prematurely senescent hMSC models. We observed m^{6}A loss during premature aging as a consequence of METTL3 downregulation. We also showed that knockout of METTL3 accelerated senescence in young hMSCs, reflected by increased SA-β-Gal staining and impaired proliferation (consistent with the findings in cancer cells (59)). Combined with the functional validations showing that METTL3 overexpression alleviated cellular senescence in prematurely senescent hMSCs, we reached a conclusion that METTL3 as well as m^{6}A play important roles in stem cell senescence. Consistent with our conclusion, a recent study has reported that METTL3 deficiency shortens lifespan in *Drosophila* (77).

In cellular models of human premature aging, m^{6}A profiling revealed declined methylation and expression levels of cell cycle-related pathways. Cell cycle arrest is a common feature in many aging contexts (65–67). As a cell cycle-related factor, MIS12 is known to interact with DSN1, NSL1, and PMF1, forming the MIS12 complex (MIS12C) that promotes chromosome segregation and kinetochore formation during mitosis (78) and thus plays critical regulatory roles in cell proliferation (68). Consistently, knockdown of MIS12 in human and chicken cells results in chromosome mis-segregation and chromosome biorientation defects (79). However, little is known about the function of MIS12 in cellular senescence. In our study, we observed significant reduction of both m^{6}A modification and *MIS12* mRNA stability in prematurely senescent hMSCs. METTL3 deficiency decreased stability of *MIS12* transcripts in hMSCs, likely due to reduced m^{6}A modifications around their stop codons preferentially recognized and bound by the m^{6}A reader IGF2BP2. Indeed, it has been reported that IGF2BP2 selectively recognizes m^{6}A-modified *MIS12* mRNA and promotes mRNA stability and

translation efficiency (23). These data offer insights into precise molecular mechanisms that underlie the regulatory roles of m^{6}A during stem cell senescence.

Epigenetic changes have a powerful influence on the aging process (41,80–84) and genetic reprogramming targeting such changes may lead to cellular rejuvenation (41). For example, partial reprogramming using the Yamanaka factors Oct4, Sox2, Klf4 and c-Myc (OSKM) restores histone modifications, including H3K9me3 and H4K20me3, and extends lifespan in a progeria mouse model (42). Rejuvenation from an epitranscriptomic aspect has not yet been reported, whereas our findings, for the first time, demonstrate that m^{6}A loss is a senescence biomarker in hMSCs and that the restoration of m^{6}A through METTL3 overexpression may rescue premature senescence phenotypes in hMSCs.

Taken together, our study puts forth a regulatory model in which IGF2BP2-mediated enhancement of *MIS12* mRNA stability is increased by METTL3-mediated m^{6}A modifications to reverse the senescent phenotypes of hMSCs. The existence of a direct molecular connection between MIS12 expression and its m^{6}A status suggests the manipulation of m^{6}A modification levels as a potential strategy for cellular rejuvenation. Our work sheds light on the poorly understood molecular mechanism of m^{6}A in aging and identifies METLL3 and MIS12 as novel biomarkers for diagnosis and candidate targets for the treatment of age-associated disorders.

DATA AVAILABILITY

RNA-seq and MeRIP-seq data generated in this study have been deposited in the Genome Sequence Archive (85) in National Genomics Data Center (86), Beijing Institute of Genomics (China National Center for Bioinformation), Chinese Academy of Sciences, under accession number HRA000206 that are publicly accessible at http://bigd.big.ac.cn/gsa-human.

SUPPLEMENTARY DATA

Supplementary Data are available at NAR Online.

ACKNOWLEDGEMENTS

We are grateful to Lei Bai, Ruijun Bai, Qun Chu, Jing Lu, Xiao Zhuo, Ying Yang and Shikun Ma for administrative assistance, Shijia Bi, Qianzhao Ji, Liangzheng Fu, Zunpeng Liu, Hongyu Li and Di Liu for their technical supports, Prof. Hailin Wang for his help in LC-MS/MS assay.

FUNDING

National Key Research and Development Program of China [2017YFA0103304]; Strategic Priority Research Program of the Chinese Academy of Sciences [XDA16010000]; National Key Research and Development Program of China [2018YFC2000100, 2017YFA0102802, 2018YFA0107203, 2019YFA0110900]; National Natural Science Foundation of China [81625009, 91749202, 81861168034, 81921006, 31671429, 91949209, 91749123, 81671377, 81822018, 81870228, 81922027, 81701388, 31800695]; Program of the Beijing Municipal Science and Technology Commission [Z191100001519005]; Beijing Natural Science Foundation [Z190019]; Beijing Municipal Commission of Health and Family Planning [PXM2018_026283_000002]; Advanced Innovation Center for Human Brain Protection [3500-1192012]; Key Research Program of the Chinese Academy of Sciences [KFZD-SW-221]; K.C. Wong Education Foundation [GJTD-2019-06, GJTD-2019-08]; Youth Innovation Promotion Association of CAS [2016093]; State Key Laboratory of Stem Cell and Reproductive Biology; State Key Laboratory of Membrane Biology.

Conflict of interest statement. None declared.

REFERENCES

1. Fu,Y., Dominissini,D., Rechavi,G. and He,C. (2014) Gene expression regulation mediated through reversible m(6)A RNA methylation. *Nat. Rev. Genet.*, **15**, 293–306.
2. Yang,X., Liu,Q.L., Xu,W., Zhang,Y.C., Yang,Y., Ju,L.F., Chen,J., Chen,Y.S., Li,K., Ren,J. *et al.* (2019) m(6)A promotes R-loop formation to facilitate transcription termination. *Cell Res.*, **29**, 1035–1038.
3. Liu,J., Dou,X., Chen,C., Chen,C., Liu,C., Xu,M.M., Zhao,S., Shen,B., Gao,Y., Han,D. *et al.* (2020) N (6)-methyladenosine of chromosome-associated regulatory RNA regulates chromatin state and transcription. *Science*, **367**, 580–586.
4. Zaccara,S., Ries,R.J. and Jaffrey,S.R. (2019) Reading, writing and erasing mRNA methylation. *Nat. Rev. Mol. Cell Biol.*, **20**, 608–624.
5. Huang,H., Weng,H. and Chen,J. (2020) The biogenesis and precise control of RNA m(6)A methylation. *Trends Genet.*, **36**, 44–52.
6. Roignant,J.Y. and Soller,M. (2017) m(6)A in mRNA: An ancient mechanism for fine-tuning gene expression. *Trends Genet.*, **33**, 380–390.
7. Niu,Y., Zhao,X., Wu,Y.S., Li,M.M., Wang,X.J. and Yang,Y.G. (2013) N6-methyl-adenosine (m6A) in RNA: an old modification with a novel epigenetic function. *Genomics Proteomics Bioinformatics*, **11**, 8–17.
8. Maity,A. and Das,B. (2016) N6-methyladenosine modification in mRNA: machinery, function and implications for health and diseases. *FEBS J.*, **283**, 1607–1630.
9. Cao,G., Li,H.B., Yin,Z. and Flavell,R.A. (2016) Recent advances in dynamic m6A RNA modification. *Open Biol*, **6**, 160003.
10. Deng,X., Su,R., Weng,H., Huang,H., Li,Z. and Chen,J. (2018) RNA N(6)-methyladenosine modification in cancers: current status and perspectives. *Cell Res.*, **28**, 507–517.
11. Ries,R.J., Zaccara,S., Klein,P., Olarerin-George,A., Namkoong,S., Pickering,B.F., Patil,D.P., Kwak,H., Lee,J.H. and Jaffrey,S.R. (2019) m(6)A enhances the phase separation potential of mRNA. *Nature*, **571**, 424–428.
12. Abakir,A., Giles,T.C., Cristini,A., Foster,J.M., Dai,N., Starczak,M., Rubio-Roldan,A., Li,M., Eleftheriou,M., Crutchley,J. *et al.* (2020) N(6)-methyladenosine regulates the stability of RNA:DNA hybrids in human cells. *Nat. Genet.*, **52**, 48–55.
13. Shi,H., Wei,J. and He,C. (2019) Where, when, and how: ontext-dependent functions of RNA methylation writers, readers, and erasers. *Mol. Cell*, **74**, 640–650.
14. Wang,P., Doxtader,K.A. and Nam,Y. (2016) Structural basis for cooperative function of Mettl3 and Mettl14 Methyltransferases. *Mol. Cell*, **63**, 306–317.
15. Wang,X., Feng,J., Xue,Y., Guan,Z., Zhang,D., Liu,Z., Gong,Z., Wang,Q., Huang,J., Tang,C. *et al.* (2016) Structural basis of N(6)-adenosine methylation by the METTL3-METTL14 complex. *Nature*, **534**, 575–578.
16. Xu,K., Yang,Y., Feng,G.H., Sun,B.F., Chen,J.Q., Li,Y.F., Chen,Y.S., Zhang,X.X., Wang,C.X., Jiang,L.Y. *et al.* (2017) Mettl3-mediated m(6)A regulates spermatogonial differentiation and meiosis initiation. *Cell Res.*, **27**, 1100–1114.
17. Lee,H., Bao,S., Qian,Y., Geula,S., Leslie,J., Zhang,C., Hanna,J.H. and Ding,L. (2019) Stage-specific requirement for Mettl3-dependent

m(6)A mRNA methylation during haematopoietic stem cell differentiation. *Nat. Cell Biol.*, **21**, 700–709.
18. Zhang,Z., Wang,M., Xie,D., Huang,Z., Zhang,L., Yang,Y., Ma,D., Li,W., Zhou,Q., Yang,Y.G. *et al.* (2018) METTL3-mediated N(6)-methyladenosine mRNA modification enhances long-term memory consolidation. *Cell Res.*, **28**, 1050–1061.
19. Batista,P.J., Molinie,B., Wang,J., Qu,K., Zhang,J., Li,L., Bouley,D.M., Lujan,E., Haddad,B., Daneshvar,K. *et al.* (2014) m(6)A RNA modification controls cell fate transition in mammalian embryonic stem cells. *Cell Stem Cell*, **15**, 707–719.
20. Vu,L.P., Pickering,B.F., Cheng,Y., Zaccara,S., Nguyen,D., Minuesa,G., Chou,T., Chow,A., Saletore,Y., MacKay,M. *et al.* (2017) The N(6)-methyladenosine (m(6)A)-forming enzyme METTL3 controls myeloid differentiation of normal hematopoietic and leukemia cells. *Nat. Med.*, **23**, 1369–1376.
21. Lin,S., Choe,J., Du,P., Triboulet,R. and Gregory,R.I. (2016) The m(6)A methyltransferase METTL3 promotes translation in human cancer cells. *Mol. Cell*, **62**, 335–345.
22. Li,T., Hu,P.S., Zuo,Z., Lin,J.F., Li,X., Wu,Q.N., Chen,Z.H., Zeng,Z.L., Wang,F., Zheng,J. *et al.* (2019) METTL3 facilitates tumor progression via an m(6)A-IGF2BP2-dependent mechanism in colorectal carcinoma. *Mol. Cancer*, **18**, 112.
23. Huang,H., Weng,H., Sun,W., Qin,X., Shi,H., Wu,H., Zhao,B.S., Mesquita,A., Liu,C., Yuan,C.L. *et al.* (2018) Recognition of RNA N(6)-methyladenosine by IGF2BP proteins enhances mRNA stability and translation. *Nat. Cell Biol.*, **20**, 285–295.
24. Dreesen,O. and Stewart,C.L. (2011) Accelerated aging syndromes, are they relevant to normal human aging? *Aging (Albany NY)*, **3**, 889–895.
25. Martin,G.M. and Oshima,J. (2000) Lessons from human progeroid syndromes. *Nature*, **408**, 263–266.
26. Ding,S.L. and Shen,C.Y. (2008) Model of human aging: recent findings on Werner's and Hutchinson-Gilford progeria syndromes. *Clin. Interv. Aging*, **3**, 431–444.
27. Burtner,C.R. and Kennedy,B.K. (2010) Progeria syndromes and ageing: what is the connection? *Nat. Rev. Mol. Cell Biol.*, **11**, 567–578.
28. Kudlow,B.A., Kennedy,B.K. and Monnat,R.J. Jr (2007) Werner and Hutchinson-Gilford progeria syndromes: mechanistic basis of human progeroid diseases. *Nat. Rev. Mol. Cell Biol.*, **8**, 394–404.
29. Wu,Z., Zhang,W., Song,M., Wang,W., Wei,G., Li,W., Lei,J., Huang,Y., Sang,Y., Chan,P. *et al.* (2018) Differential stem cell aging kinetics in Hutchinson-Gilford progeria syndrome and Werner syndrome. *Protein Cell*, **9**, 333–350.
30. Zhang,H., Sun,L., Wang,K., Wu,D., Trappio,M., Witting,C. and Cao,K. (2016) Loss of H3K9me3 correlates with ATM activation and histone H2AX phosphorylation deficiencies in hutchinson-gilford progeria syndrome. *PLoS One*, **11**, e0167454.
31. Liu,G.-H., Barkho,B.Z., Ruiz,S., Diep,D., Qu,J., Yang,S.-L., Panopoulos,A.D., Suzuki,K., Kurian,L., Walsh,C. *et al.* (2011) Recapitulation of premature ageing with iPSCs from Hutchinson–Gilford progeria syndrome. *Nature*, **472**, 221–225.
32. Zhang,W., Li,J., Suzuki,K., Qu,J., Wang,P., Zhou,J., Liu,X., Ren,R., Xu,X., Ocampo,A. *et al.* (2015) Aging stem cells. A Werner syndrome stem cell model unveils heterochromatin alterations as a driver of human aging. *Science*, **348**, 1160–1163.
33. Ren,X., Lim,S., Ji,Z., Yuh,J., Peng,V., Smith,M.T. and Zhang,L. (2011) Comparison of proliferation and genomic instability responses to WRN silencing in hematopoietic HL60 and TK6 cells. *PLoS One*, **6**, e14546.
34. Shamanna,R.A., Croteau,D.L., Lee,J.H. and Bohr,V.A. (2017) Recent advances in understanding werner syndrome. *F1000Res*, **6**, 1779.
35. McCord,R.P., Nazario-Toole,A., Zhang,H., Chines,P.S., Zhan,Y., Erdos,M.R., Collins,F.S., Dekker,J. and Cao,K. (2013) Correlated alterations in genome organization, histone methylation, and DNA-lamin A/C interactions in Hutchinson-Gilford progeria syndrome. *Genome Res.*, **23**, 260–269.
36. Bohr,V.A., Dianov,G., Balajee,A., May,A. and Orren,D.K. (1998) DNA repair and transcription in human premature aging disorders. *J. Investig. Dermatol. Symp. Proc.*, **3**, 11–13.
37. Burla,R., La Torre,M., Merigliano,C., Verni,F. and Saggio,I. (2018) Genomic instability and DNA replication defects in progeroid syndromes. *Nucleus (Calcutta)*, **9**, 368–379.
38. Buchwalter,A. and Hetzer,M.W. (2017) Nucleolar expansion and elevated protein translation in premature aging. *Nat. Commun.*, **8**, 328.
39. de Boer,J., Andressoo,J.O., de Wit,J., Huijmans,J., Beems,R.B., van Steeg,H., Weeda,G., van der Horst,G.T., van Leeuwen,W., Themmen,A.P. *et al.* (2002) Premature aging in mice deficient in DNA repair and transcription. *Science*, **296**, 1276–1279.
40. Chen,Z., Chang,W.Y., Etheridge,A., Strickfaden,H., Jin,Z., Palidwor,G., Cho,J.H., Wang,K., Kwon,S.Y., Dore,C. *et al.* (2017) Reprogramming progeria fibroblasts re-establishes a normal epigenetic landscape. *Aging Cell*, **16**, 870–887.
41. Zhang,W., Qu,J., Liu,G.H. and Belmonte,J.C.I. (2020) The ageing epigenome and its rejuvenation. *Nat. Rev. Mol. Cell Biol.*, **21**, 137–150.
42. Ocampo,A., Reddy,P., Martinez-Redondo,P., Platero-Luengo,A., Hatanaka,F., Hishida,T., Li,M., Lam,D., Kurita,M., Beyret,E. *et al.* (2016) In vivo amelioration of age-associated hallmarks by partial reprogramming. *Cell*, **167**, 1719–1733.
43. Shen,L., Liang,Z. and Yu,H. (2017) Dot blot analysis of N6-methyladenosine RNA modification levels. *Bio-Protocol*, **7**, 1–5.
44. Zhang,C., Chen,Y., Sun,B., Wang,L., Yang,Y., Ma,D., Lv,J., Heng,J., Ding,Y., Xue,Y. *et al.* (2017) m(6)A modulates haematopoietic stem and progenitor cell specification. *Nature*, **549**, 273–276.
45. Dominissini,D., Moshitch-Moshkovitz,S., Salmon-Divon,M., Amariglio,N. and Rechavi,G. (2013) Transcriptome-wide mapping of N(6)-methyladenosine by m(6)A-seq based on immunocapturing and massively parallel sequencing. *Nat. Protoc.*, **8**, 176–189.
46. Han,D., Liu,J., Chen,C., Dong,L., Liu,Y., Chang,R., Huang,X., Liu,Y., Wang,J., Dougherty,U. *et al.* (2019) Anti-tumour immunity controlled through mRNA m(6)A methylation and YTHDF1 in dendritic cells. *Nature*, **566**, 270–274.
47. Liu,J., Eckert,M.A., Harada,B.T., Liu,S.M., Lu,Z., Yu,K., Tienda,S.M., Chryplewicz,A., Zhu,A.C., Yang,Y. *et al.* (2018) m(6)A mRNA methylation regulates AKT activity to promote the proliferation and tumorigenicity of endometrial cancer. *Nat. Cell Biol.*, **20**, 1074–1083.
48. Wang,X., Lu,Z., Gomez,A., Hon,G.C., Yue,Y., Han,D., Fu,Y., Parisien,M., Dai,Q., Jia,G. *et al.* (2014) N6-methyladenosine-dependent regulation of messenger RNA stability. *Nature*, **505**, 117–120.
49. Wang,C.X., Cui,G.S., Liu,X., Xu,K., Wang,M., Zhang,X.X., Jiang,L.Y., Li,A., Yang,Y., Lai,W.Y. *et al.* (2018) METTL3-mediated m6A modification is required for cerebellar development. *PLoS Biol.*, **16**, e2004880.
50. Liu,J., Li,K., Cai,J., Zhang,M., Zhang,X., Xiong,X., Meng,H., Xu,X., Huang,Z., Peng,J. *et al.* (2020) Landscape and regulation of m(6)A and m(6)Am methylome across human and mouse tissues. *Mol. Cell*, **77**, 426–440.
51. Wen,J., Lv,R., Ma,H., Shen,H., He,C., Wang,J., Jiao,F., Liu,H., Yang,P., Tan,L. *et al.* (2018) Zc3h13 regulates nuclear RNA m(6)A methylation and mouse embryonic stem cell self-renewal. *Mol. Cell*, **69**, 1028–1038.
52. Deng,L., Ren,R., Liu,Z., Song,M., Li,J., Wu,Z., Ren,X., Fu,L., Li,W., Zhang,W. *et al.* (2019) Stabilizing heterochromatin by DGCR8 alleviates senescence and osteoarthritis. *Nat. Commun.*, **10**, 3329.
53. Bi,S., Liu,Z., Wu,Z., Wang,Z., Liu,X., Wang,S., Ren,J., Yao,Y., Zhang,W., Song,M. *et al.* (2020) SIRT7 antagonizes human stem cell aging as a heterochromatin stabilizer. *Protein Cell*, **11**, 483–504.
54. Liu,G.H., Suzuki,K., Qu,J., Sancho-Martinez,I., Yi,F., Li,M., Kumar,S., Nivet,E., Kim,J., Soligalla,R.D. *et al.* (2011) Targeted gene correction of laminopathy-associated LMNA mutations in patient-specific iPSCs. *Cell Stem Cell*, **8**, 688–694.
55. Kubben,N., Zhang,W., Wang,L., Voss,T.C., Yang,J., Qu,J., Liu,G.H. and Misteli,T. (2016) Repression of the antioxidant NRF2 pathway in premature aging. *Cell*, **165**, 1361–1374.
56. Hu,H., Ji,Q., Song,M., Ren,J., Liu,Z., Wang,Z., Liu,X., Yan,K., Hu,J., Jing,Y. *et al.* (2020) ZKSCAN3 counteracts cellular senescence by stabilizing heterochromatin. *Nucleic Acids Res.*, **48**, 6001–6018.
57. Linder,B., Grozhik,A.V., Olarerin-George,A.O., Meydan,C., Mason,C.E. and Jaffrey,S.R. (2015) Single-nucleotide-resolution mapping of m6A and m6Am throughout the transcriptome. *Nat. Methods*, **12**, 767–772.
58. Dominissini,D., Moshitch-Moshkovitz,S., Schwartz,S., Salmon-Divon,M., Ungar,L., Osenberg,S., Cesarkas,K.,

Jacob-Hirsch,J., Amariglio,N., Kupiec,M. *et al.* (2012) Topology of the human and mouse m6A RNA methylomes revealed by m6A-seq. *Nature*, **485**, 201–206.
59. Liu,L., Wang,J., Sun,G., Wu,Q., Ma,J., Zhang,X., Huang,N., Bian,Z., Gu,S., Xu,M. *et al.* (2019) m(6)A mRNA methylation regulates CTNNB1 to promote the proliferation of hepatoblastoma. *Mol. Cancer*, **18**, 188.
60. Pandit,S., Wang,D. and Fu,X.D. (2008) Functional integration of transcriptional and RNA processing machineries. *Curr. Opin. Cell Biol.*, **20**, 260–265.
61. Rajani,D.K., Walch,M., Martinvalet,D., Thomas,M.P. and Lieberman,J. (2012) Alterations in RNA processing during immune-mediated programmed cell death. *Proc. Natl. Acad. Sci. USA*, **109**, 8688–8693.
62. Naro,C., Bielli,P., Pagliarini,V. and Sette,C. (2015) The interplay between DNA damage response and RNA processing: the unexpected role of splicing factors as gatekeepers of genome stability. *Front Genet*, **6**, 142.
63. Berger,S.L. (2002) Histone modifications in transcriptional regulation. *Curr. Opin. Genet. Dev.*, **12**, 142–148.
64. Ito,T. (2007) Role of histone modification in chromatin dynamics. *J. Biochem.*, **141**, 609–614.
65. Chandler,H. and Peters,G. (2013) Stressing the cell cycle in senescence and aging. *Curr. Opin. Cell Biol.*, **25**, 765–771.
66. Lopez-Otin,C., Blasco,M.A., Partridge,L., Serrano,M. and Kroemer,G. (2013) The hallmarks of aging. *Cell*, **153**, 1194–1217.
67. van Deursen,J.M. (2014) The role of senescent cells in ageing. *Nature*, **509**, 439–446.
68. Abe-Kanoh,N., Kunisue,N., Myojin,T., Chino,A., Munemasa,S., Murata,Y., Satoh,A., Moriya,H. and Nakamura,Y. (2019) Yeast screening system reveals the inhibitory mechanism of cancer cell proliferation by benzyl isothiocyanate through down-regulation of Mis12. *Sci. Rep.*, **9**, 8866.
69. Geula,S., Moshitch-Moshkovitz,S., Dominissini,D., Mansour,A.A., Kol,N., Salmon-Divon,M., Hershkovitz,V., Peer,E., Mor,N., Manor,Y.S. *et al.* (2015) Stem cells. m6A mRNA methylation facilitates resolution of naive pluripotency toward differentiation. *Science*, **347**, 1002–1006.
70. Wang,Q., Chen,C., Ding,Q., Zhao,Y., Wang,Z., Chen,J., Jiang,Z., Zhang,Y., Xu,G., Zhang,J. *et al.* (2020) METTL3-mediated m(6)A modification of HDGF mRNA promotes gastric cancer progression and has prognostic significance. *Gut*, **69**, 1193–1205.
71. De Jesus,D.F., Zhang,Z., Kahraman,S., Brown,N.K., Chen,M., Hu,J., Gupta,M.K., He,C. and Kulkarni,R.N. (2019) m(6)A mRNA methylation regulates human β-Cell biology in physiological states and in type 2 diabetes. *Nat Metab*, **1**, 765–774.
72. Chen,X., Yu,C., Guo,M., Zheng,X., Ali,S., Huang,H., Zhang,L., Wang,S., Huang,Y., Qie,S. *et al.* (2019) Down-Regulation of m6A mRNA methylation is involved in dopaminergic neuronal death. *ACS Chem. Neurosci.*, **10**, 2355–2363.
73. Han,M., Liu,Z., Xu,Y., Liu,X., Wang,D., Li,F., Wang,Y. and Bi,J. (2020) Abnormality of m6A mRNA methylation is involved in Alzheimer's disease. *Front. Neurosci.*, **14**, 98.
74. Tang,C., Xie,Y., Yu,T., Liu,N., Wang,Z., Woolsey,R.J., Tang,Y., Zhang,X., Qin,W., Zhang,Y. *et al.* (2020) m(6)A-dependent biogenesis of circular RNAs in male germ cells. *Cell Res.*, **30**, 211–228.
75. Dorn,L.E., Lasman,L., Chen,J., Xu,X., Hund,T.J., Medvedovic,M., Hanna,J.H., van Berlo,J.H. and Accornero,F. (2019) The N(6)-Methyladenosine mRNA Methylase METTL3 controls cardiac homeostasis and hypertrophy. *Circulation*, **139**, 533–545.
76. Min,K.W., Zealy,R.W., Davila,S., Fomin,M., Cummings,J.C., Makowsky,D., McDowell,C.H., Thigpen,H., Hafner,M., Kwon,S.H. *et al.* (2018) Profiling of m6A RNA modifications identified an age-associated regulation of AGO2 mRNA stability. *Aging Cell*, **17**, e12753.
77. Kan,L., Ott,S., Joseph,B., Park,E.S., Dai,C., Kleiner,R., Claridge-Chang,A. and Lai,E.C. (2020) A neural m6A/YTHDF pathway is required for learning and memory in Drosophila. bioRxiv doi: https://doi.org/10.1101/2020.03.07.982090 07 March 2020, preprint: not peer reviewed.
78. Goshima,G., Kiyomitsu,T., Yoda,K. and Yanagida,M. (2003) Human centromere chromatin protein hMis12, essential for equal segregation, is independent of CENP-A loading pathway. *J. Cell Biol.*, **160**, 25–39.
79. Desai,A., Fukagawa,T., Hori,T., Cheeseman,I.M. and Kline,S.L. (2006) The human Mis12 complex is required for kinetochore assembly and proper chromosome segregation. *J. Cell Biol.*, **173**, 9–17.
80. Rando,T.A. and Chang,H.Y. (2012) Aging, rejuvenation, and epigenetic reprogramming: resetting the aging clock. *Cell*, **148**, 46–57.
81. Sen,P., Shah,P.P., Nativio,R. and Berger,S.L. (2016) Epigenetic mechanisms of longevity and aging. *Cell*, **166**, 822–839.
82. Pal,S. and Tyler,J.K. (2016) Epigenetics and aging. *Sci Adv*, **2**, e1600584.
83. Ren,R., Ocampo,A., Liu,G.H. and Izpisua Belmonte,J.C. (2017) Regulation of stem cell aging by metabolism and epigenetics. *Cell Metab.*, **26**, 460–474.
84. Booth,L.N. and Brunet,A. (2016) The aging epigenome. *Mol. Cell*, **62**, 728–744.
85. Wang,Y., Song,F., Zhu,J., Zhang,S., Yang,Y., Chen,T., Tang,B., Dong,L., Ding,N., Zhang,Q. *et al.* (2017) GSA: genome sequence archive. *Genomics Proteomics Bioinformatics*, **15**, 14–18.
86. National Genomics Data Center Members and Partners (2020) Database resources of the national genomics data center in 2020. *Nucleic Acids Res.*, **48**, D24–D33.